

# MAUS: The MICE Analysis User Software

---

R. Asfandiyarov,<sup>a</sup> R. Bayes,<sup>b</sup> V. Blackmore,<sup>c</sup> M. Bogomilov,<sup>d</sup> D. Colling,<sup>c</sup> A.J. Dobbs,<sup>c</sup> F. Drielsma,<sup>a</sup> M. Ellis,<sup>c</sup> M. Fedorov,<sup>e</sup> P. Franchini,<sup>f</sup> R. Gardener,<sup>g</sup> J.R. Greis,<sup>f</sup> P.M. Hanlet,<sup>h</sup> C. Heidt,<sup>i</sup> C. Hunt,<sup>c</sup> G. Kafka,<sup>h</sup> Y. Karadzhov,<sup>a</sup> A. Kurup,<sup>c</sup> P. Kyberd,<sup>g</sup> M. Littlefield,<sup>g</sup> A. Liu,<sup>j</sup> K.L. Long,<sup>c,n</sup> D. Maletic,<sup>k</sup> J. Martyniak,<sup>c</sup> S. Middleton,<sup>c</sup> T. Mohayai,<sup>g</sup> J.C. Nugent,<sup>b</sup> E. Overton,<sup>l</sup> V. Pec,<sup>l</sup> C.E. Pidcott,<sup>f</sup> D. Rajaram,<sup>h,1</sup> C.T. Rogers,<sup>n</sup> M. Savic,<sup>k</sup> I. Taylor,<sup>f</sup> Y.T. Torun,<sup>h</sup> C.D. Tunnell,<sup>m</sup> M.A. Uchida,<sup>c</sup> V. Verguilov,<sup>a</sup> K. Walaron,<sup>b</sup> S. Wilbur<sup>l</sup>

<sup>a</sup>DPNC, section de Physique, Université de Genève, Geneva, Switzerland

<sup>b</sup>School of Physics and Astronomy, Kelvin Building, The University of Glasgow, Glasgow, UK

<sup>c</sup>Department of Physics, Blackett Laboratory, Imperial College London, London, UK

<sup>d</sup>Department of Atomic Physics, St. Kliment Ohridski University of Sofia, Sofia, Bulgaria

<sup>e</sup>Radboud University of Nijmegen, Netherlands

<sup>f</sup>Department of Physics, University of Warwick, Coventry, UK

<sup>g</sup>Brunel University, Uxbridge, UK

<sup>h</sup>Physics Department, Illinois Institute of Technology, Chicago, IL, USA

<sup>i</sup>University of California, Riverside, CA, USA

<sup>j</sup>Fermilab, Batavia, IL, USA

<sup>k</sup>Institute of Physics, University of Belgrade, Serbia

<sup>l</sup>Department of Physics and Astronomy, University of Sheffield, Sheffield, UK

<sup>m</sup>Department of Physics, University of Oxford, Denys Wilkinson Building, Oxford, UK

<sup>n</sup>STFC Rutherford Appleton Laboratory, Harwell Oxford, Didcot, UK

E-mail: [durga@fnal.gov](mailto:durga@fnal.gov)

**ABSTRACT:** The Muon Ionization Cooling Experiment (MICE) collaboration has developed the MICE Analysis User Software (MAUS) to simulate and analyze experimental data. It serves as the primary codebase for the experiment, providing for offline batch simulation and reconstruction as well as online data quality checks. The software provides both traditional particle-physics functionalities such as track reconstruction and particle identification, and accelerator physics functions, such as calculating transfer matrices and emittances. The code design is object orientated, but has a top-level structure based on the Map-Reduce model. This allows for parallelization to support live data reconstruction during data-taking operations. MAUS allows users to develop in either Python or C++ and provides APIs for both. Various software engineering practices from industry are also used to ensure correct and maintainable code, including style, unit and integration tests, continuous integration and load testing, code reviews, and distributed version control. The software framework and the simulation and reconstruction capabilities are described.

**KEYWORDS:** MICE; Ionization Cooling; Software; Reconstruction; Simulation

---

<sup>1</sup>Corresponding author.

---

## Contents

<b>1</b>	<b>Introduction</b>	<b>2</b>
1.1	The MICE experiment	2
1.2	Software requirements	3
<b>2</b>	<b>MAUS</b>	<b>3</b>
2.1	Code design	3
2.2	Data structure	6
2.2.1	Physics data	6
2.2.2	Top level data organisation	12
2.3	Data flow	12
2.4	Testing	12
<b>3</b>	<b>Monte Carlo</b>	<b>14</b>
3.1	Beam generation	14
3.2	Geant4	14
3.3	Geometry	15
3.4	Tracking, field maps and beam optics	15
3.5	Detector response and digitization	16
<b>4</b>	<b>Reconstruction</b>	<b>16</b>
4.1	Time of flight	16
4.2	Scintillating fiber trackers	17
4.3	KL calorimeter	17
4.4	Electron-muon ranger	17
4.5	Cherenkov	18
4.6	Global reconstruction	18
4.6.1	Global track matching	18
4.6.2	Global PID	18
4.7	Online reconstruction	19
<b>5</b>	<b>Summary</b>	<b>19</b>

---

# 1 Introduction

## 1.1 The MICE experiment

The Muon Ionization Cooling Experiment (MICE) sited at the STFC Rutherford Appleton Laboratory (RAL) has delivered the first demonstration of muon ionization cooling [1] – the reduction of the phase-space of muon beams. Muon-beam cooling is essential for future facilities based on muon acceleration, such as the Neutrino Factory or Muon Collider [2, 3]. The experiment was designed to be built and operated in a staged manner. In the first stage, the muon beamline was commissioned [4] and characterized [5]. The configuration shown in figure 1 was used to study the factors that determine the performance of an ionization-cooling channel and to observe for the first time the reduction in transverse emittance of a muon beam.

The MICE Muon Beam line is described in detail in [4]. There are 5 different detector systems present on the beamline: time-of-flight (TOF) scintillators [6], threshold Cherenkov (Ckov) counters [7], scintillating fiber trackers [8], a sampling calorimeter (KL) [5], and the Electron Muon Ranger (EMR) – a totally active scintillating calorimeter [9]. The TOF detector system consists of three detector stations, TOF0, TOF1 and TOF2, each composed of two orthogonal layers of scintillator bars. The TOF system is used to determine particle identification (PID) via the time-of-flight between the stations. Each station also provides a low resolution image of the beam profile. The Ckov system consists of two aerogel threshold Cherenkov stations, CkovA and CkovB. The KL and EMR detectors, the former using scintillating fibers embedded in lead sheets, and the latter scintillating bars, form the downstream calorimeter system.

The tracker system consists of two scintillating fiber detectors, one upstream of the MICE cooling cell, the other downstream, in order to measure the change in emittance across the cooling cell. Each detector consists of 5 stations, each station in having 3 fiber planes, allowing precision measurement of momentum and position to be made on a particle-by-particle basis.

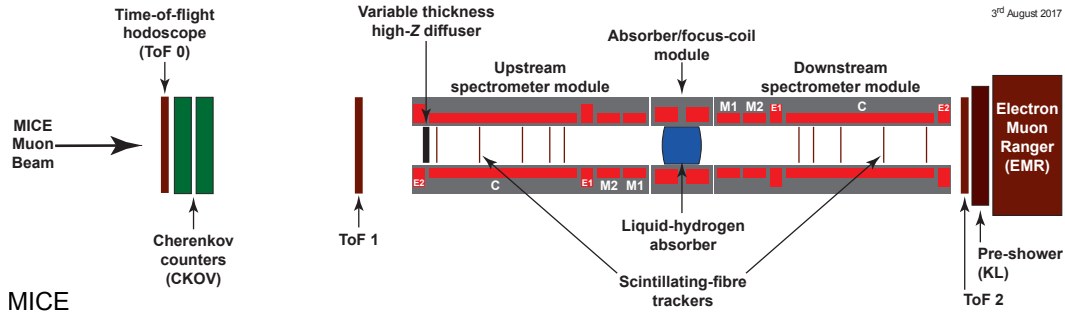


**Figure 1.** Schematic diagram of the final configuration of the MICE experiment. The red rectangles represent the coils of the spectrometer solenoids and focus coil. The individual coils of the spectrometer solenoids are labelled E1, C, E2, M1 and M2. The various detectors are also represented.

## 1.2 Software requirements

The MICE software must serve both the accelerator-physics and the particle-physics needs of the experiment. Traditional particle-physics functionality includes reconstructing particle tracks, identifying them, and simulating the response from various detectors, while the accelerator-physics aspect includes the calculation of transfer matrices and Twiss parameters and propagating the beam envelopes. All of these items require a detailed description of the beamline, the geometries of the detectors, and the magnetic fields, as well as functionality to simulate the various detectors and reconstruct the detector outputs.

Given the complexity and the time-scale of the experiment, it was essential to ensure that the software can be maintained over the long-term. Good performance was also important in order to ensure that the software can reconstruct data with sufficient speed to support live online monitoring of the experiment.

## 2 MAUS

The MICE Analysis User Software (MAUS) [10] is the collaboration’s simulation, reconstruction, and analysis software framework. MAUS provides a Monte Carlo (MC) simulation of the experiment, reconstruction of tracks and identification of particles from simulations and real data, and provides monitoring and diagnostics while running the experiment.

Installation is performed via a set of shell scripts with SCons [11] as the build tool. The codebase is maintained with the GNU Bazaar revision control system [12] and is hosted on Launchpad [13]. MAUS has a number of dependencies on standard packages such as Python, ROOT [14] and Geant4 [15] which are built as "third party" external libraries during the installation process. The officially supported platform is Scientific Linux 6 [16] though developers have successfully built on CentOS [17], Fedora [18], and Ubuntu [19] distributions.

Each of the MICE detector systems, described in section 1.1, is represented within MAUS. Their data structures are described in section 2.2 and their simulation and reconstruction algorithms in sections 3 and 4. MAUS also provides “global” reconstruction routines, which combine data from individual detector systems to identify particle species by the likelihood method and a global track fit. These algorithms are also described in section 4.

### 2.1 Code design

MAUS is written in a mixture of Python and C++. C++ is used for complex or low-level algorithms where processing time is important, while Python is used for simple or high-level algorithms where development time is a more stringent requirement. Developers are allowed to write in either Python or C++ and Python bindings to C++ are handled through internal abstractions. In practice, all the reconstruction modules are written in C++ but support is provided for legacy modules written in Python.

MAUS has an Application Programming Interface (API) that provides a framework on which developers can hang individual routines. The MAUS API provides MAUS developers with a well-

defined environment for developing reconstruction code, while allowing independent development of the back-end and code-sharing of common elements, such as error handling and data-wrangling.

The MAUS data processing model is inspired by the Map-Reduce framework [20], which forms the core of the API design. Map-Reduce, illustrated in figure 2 is a useful model for parallelizing data processing on a large scale. For MAUS, the API was simplified to use *transformers* in place of maps, though these modules have retained the name *map*. A map process takes a single object as an input, which remains unaltered, and returns a new object as the output, whereas a transformer process alters the input object in place (in the case of MAUS this object is the *spill* class, see Section 2.2).

A *Module* is the basic building block of the MAUS API framework. Four types of module exist within MAUS:

1. **Inputters** generate input data either by reading data from files or sockets, or by generating an input beam;
2. **Mappers** modify the input data, for example by reconstructing signals from detectors, or tracking particles to generate MC hits;
3. **Reducers** collate the mapped data and allow functionality that requires access to the entire data set; and
4. **Outputters** save the data either by streaming over a socket or writing to disk.

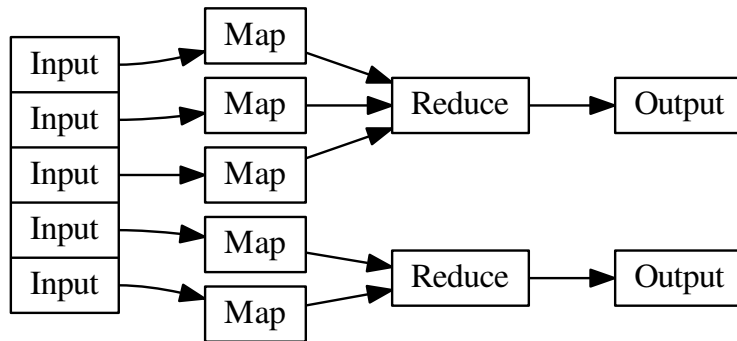


**Figure 2.** A Map-Reduce framework.

Each module type follows a common, extensible, object-orientated class heirarchy, shown for the case of the map and reduce modules in figure 3.

There are some objects that sit outside the scope of this modular framework but are nevertheless required by several of the modules. For instance, the detector geometries, magnetic fields, and calibrations are required by the reconsruction and simulation modules, and objects such as the electronics-cabling maps are required in order to unpack data from the data acquisition (DAQ) source,

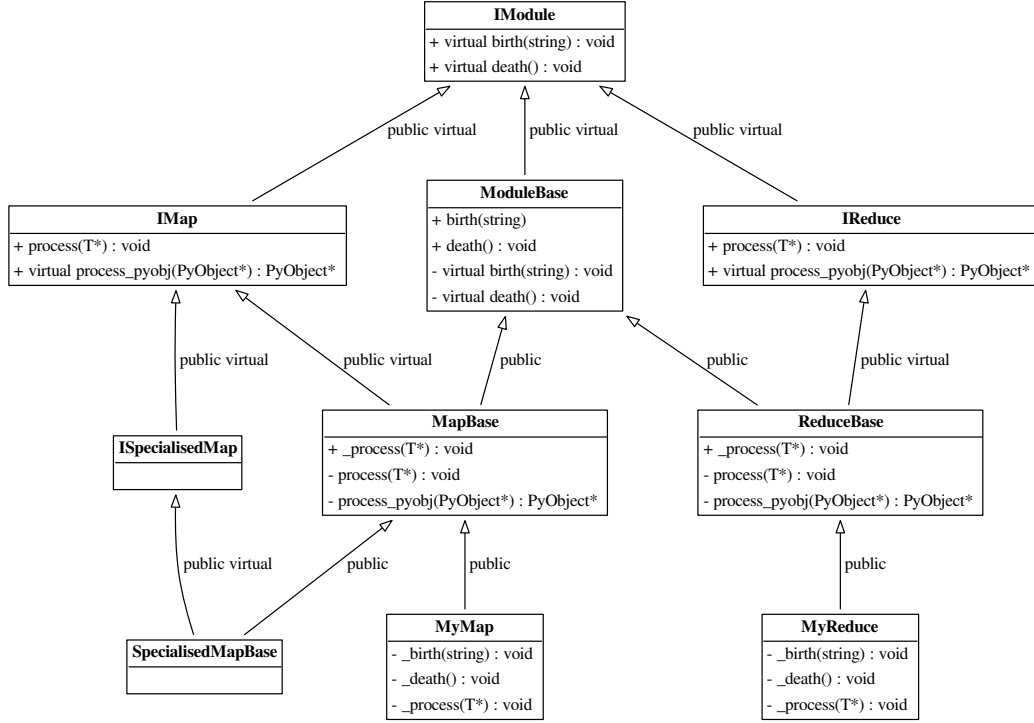


**Figure 3.** The MAUS API class hierarchy for Map and Reduce modules. The input and output modules follow related designs.  $T$  represents a templated argument. “+” indicates the introduction of a virtual void method, defining an interface, while “-” indicates that a class implements that method, fulfilling that aspect of the interface. The *process\_pyobj* functions are the main entry points for Python applications, and *process* the entry points for C++ applications. The framework can be extended as many times as necessary, as exemplified by the “SpecialisedMap” classes.

and error handling functionality is required by all of the modules. All these objects are accessed through a static singleton *globals* class.

MAUS has two execution concepts. A *job* refers to a single execution of the code, while a *run* refers to the processing of data for a DAQ run or MC run. A job may contain many runs. Since data are typically accessed from a single source and written to a single destination, Inputters and Outputters are initialized and destroyed at the beginning and end of a job. On the other hand, Mappers and Reducers are initialized at the beginning of a run in order to allow run-specific information such as electronics cabling maps, fields, and calibrations to be loaded.

The principal data type in MAUS, which is passed from module to module, is the *spill*. A single spill corresponds to data from the particle burst associated with a dip of the MICE target [4]. A spill lasts up to  $\sim 3$  ms and contains several DAQ triggers. Data from a given trigger define a single MICE *event*. In the language of the Input-Map-Reduce-Output framework, an Input module creates

an instance of spill data, a Map module processes the spill (simulating, reconstructing, etc.), a Reduce module acts on a collection of spills when all the mappers finish, and finally an Output module records the data to a given file format.

Modules can exchange spill data either as C++ pointers or JSON [21] objects. In Python, the data format can be changed by using a converter module, and in C++ mappers are templated to a MAUS data type and an API handles any necessary conversion to that type (see Fig. 3).

Data contained within the MAUS data structure (see Section 2.2) can be saved to permanent storage in one of two formats. The default data format is a ROOT [14] binary and the secondary format is JSON. ROOT is a standard high-energy physics analysis package, distributed with MAUS, through which many of the analyses on MICE are performed. Each spill is stored as a single entry in a ROOT TTree object. JSON is an ASCII data-tree format. Specific JSON parsers are available – for example, the Python *json* library, and the C++ *JsonCpp* [22] parser come prepackaged with MAUS.

In addition to storing the output from the Map modules, MAUS is also capable of storing the data produced by *Reducer* modules using a special *Image* class. This class is used by *Reducers* to store images of monitoring histograms, efficiency plots, etc. *Image* data may only be saved in JSON format.

## 2.2 Data structure

### 2.2.1 Physics data

At the top of the MAUS data structure is the spill class which contains all the data from the simulation, raw real data and the reconstructed data. The spill is passed between modules and written to permanent storage. The data within a spill is organized into arrays of three possible event types: an *MCEvent* contains data representing the simulation of a single particle traversing the experiment and the simulated detector responses; a *DAQEvent* corresponds to the real data for a single trigger; and a *ReconEvent* corresponds to the data reconstructed for a single particle event (arising either from a Monte Carlo(MC) particle or a real data trigger). These different branches of the MAUS data structure are shown diagrammatically in figures 4–9.

The sub-structure of the the MC event class is shown in figure 5. The class is subdivided into events containing detector hits (energy deposited, position, momentum) for each of the MICE detectors (see Section 1.1). The event also contains information about the primary particle that created the hits in the detectors.

The sub-structure of the the reconstruction event class is shown in figure 6. The class is subdivided into events representing each of the MICE detectors, together with the data from the trigger, and data for the global event reconstruction. Each detector class and the global reconstruction class has several further layers of reconstruction data. This is shown in figures 7–9.

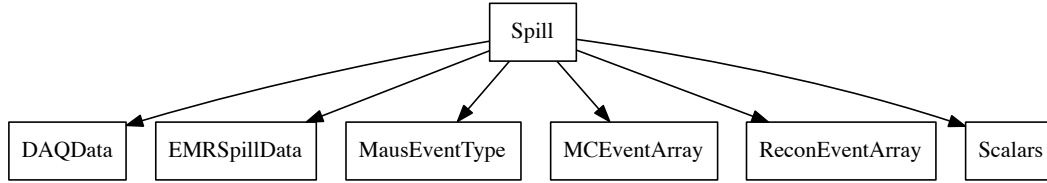


**Figure 4.** The MAUS output structure for a spill event. The label in each box is the name of the C++ class.

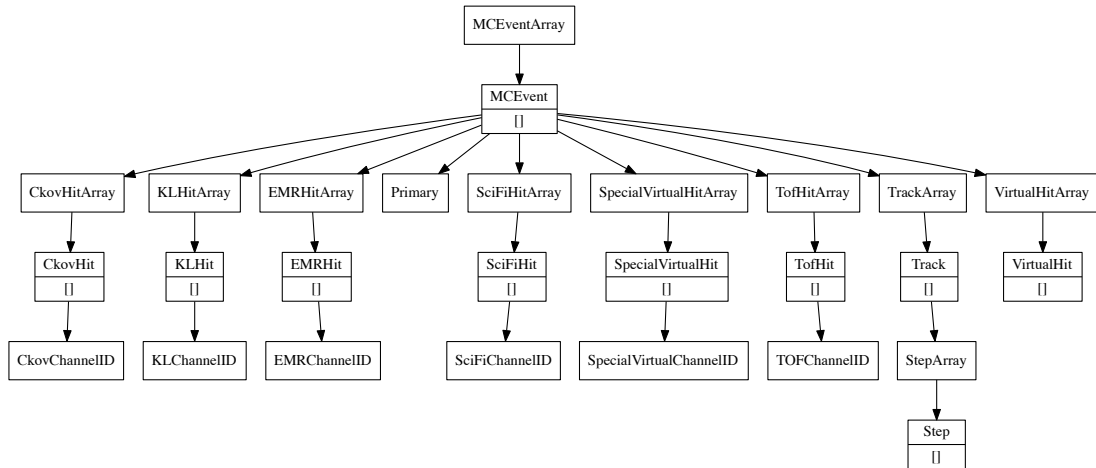


**Figure 5.** The MAUS data structure for MC events. The label in each box is the name of the C++ class and [] indicates that child objects are array items.



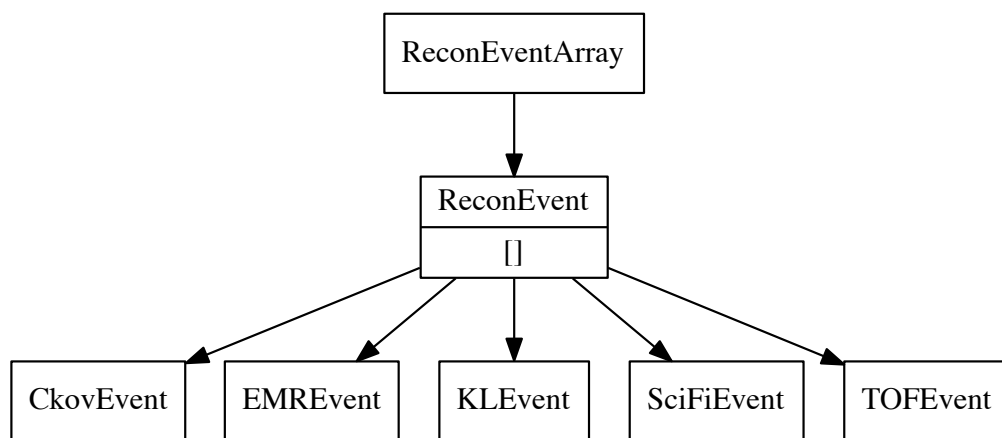


**Figure 6.** The MAUS data structure for reconstructed events. The label in each box is the name of the C++ class.

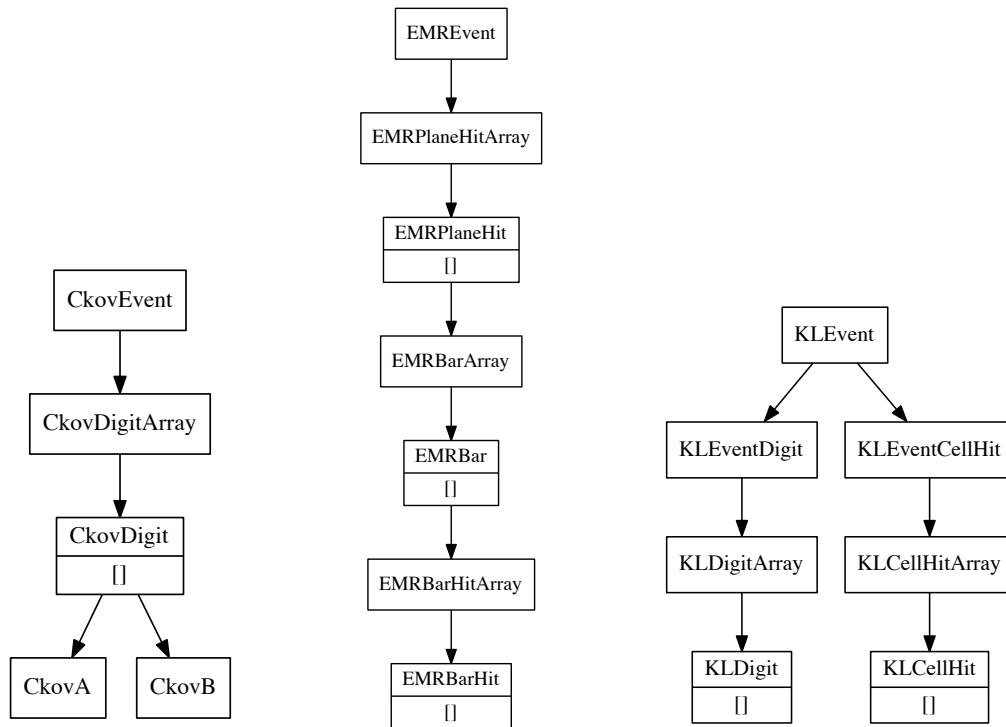


**Figure 7.** The MAUS data structure for CKOV (left), EMR (middle) and KL (right) reconstructed events. The label in each box is the name of the C++ class [] indicates that child objects are array items.

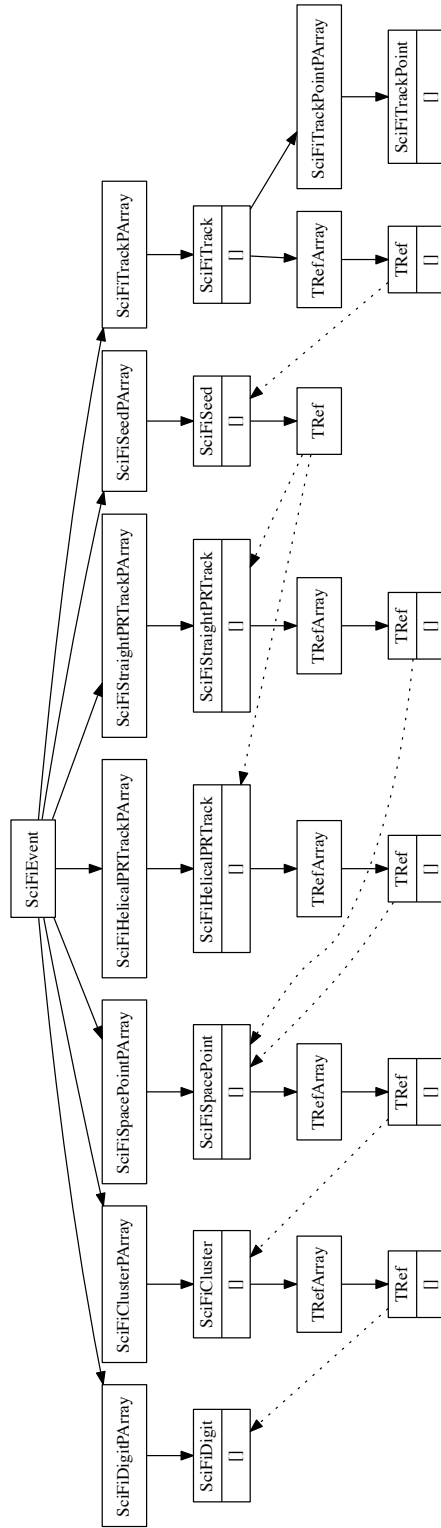


**Figure 8.** The MAUS data structure for the tracker. The label in each box is the name of the C++ class and [] indicates that child objects are array items.

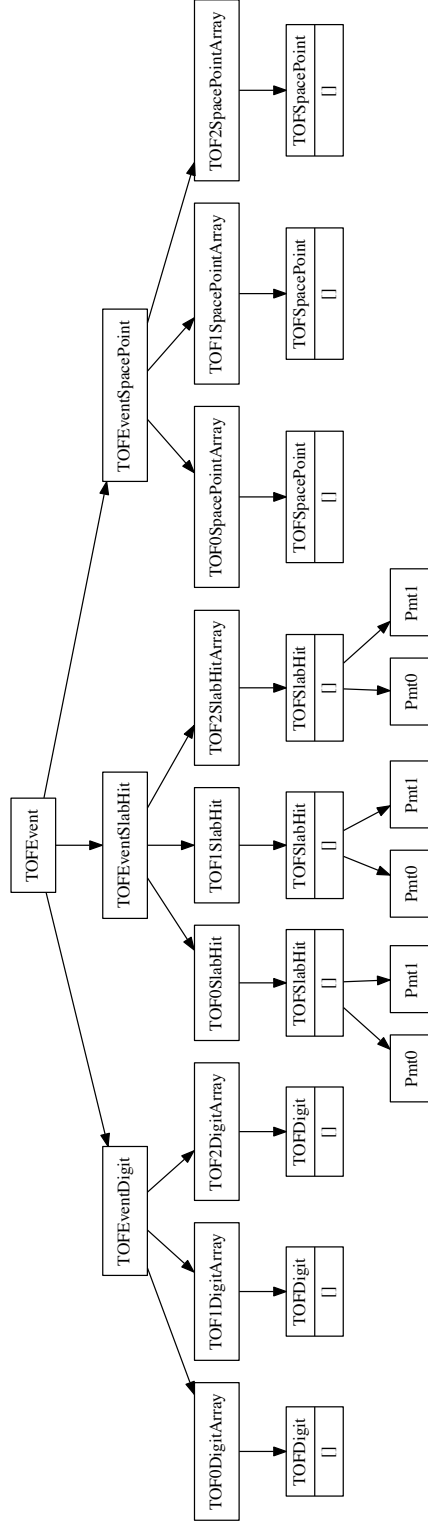


**Figure 9.** The MAUS data structure for the TOFs. The label in each box is the name of the C++ class and [] indicates that child objects are array items.

## 2.2.2 Top level data organisation

In addition to the spill data, MAUS also contains structures for storing supplementary information for each run and job. These are referred to as *JobHeader* and *JobFooter*, and *RunHeader* and *RunFooter*. The former represents data from the start and end of a job, such as the MAUS release version used to create it, and the latter data from the start and end of a run, such as the geometry ID used for the data processing. This may be saved to permanent storage along with the spill.

In order to interface with ROOT, particularly in order to save data in the ROOT format, thin wrappers for each of the top level classes, and a templated base class, were introduced. This allows the ROOT TTree, in which the output data is stored (see Section 2.2.1), to be given a single memory address to read from. The wrapper for Spill is called *Data*, while for each of *RunHeader*, *RunFooter*, *JobHeader* and *JobFooter*, the respective wrapper class is just given the original class name with “Data” appended, e.g., *RunHeaderData*. The base class for each of the wrappers is called *MAUSEvent*. The class hierarchy is illustrated in Figure 10.

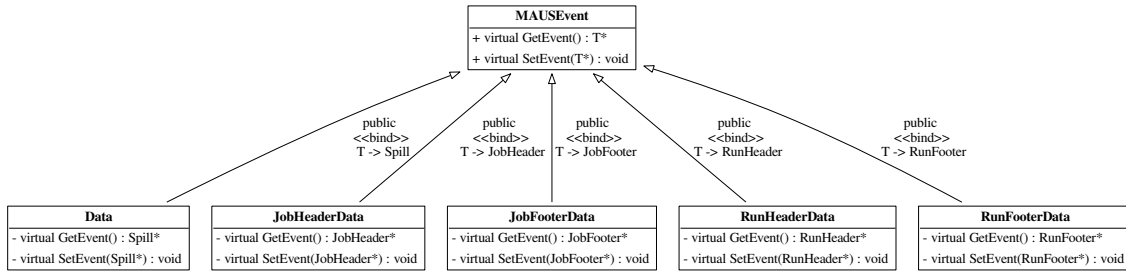


**Figure 10.** Class hierarchy for the wrappers and base class of the top-level classes of the MAUS data structure.

## 2.3 Data flow

The MAUS data flow, showing the reconstruction chain for data originating from MC or real data, is depicted in figure 11. Each item in the diagram is implemented as an individual module. The data flow is grouped into three principal areas: the simulation data flow used to generate digits (electronics signals) from particle tracking; the real data flow used to generate digits from real detector data; and the reconstruction data flow which illustrates how digits are built into higher level objects and converted to parameters of interest. The reconstruction data flow is the same for digits from real data and simulation. In the case of real data, separate input modules are provided to read either directly from the DAQ, or from archived data stored on disk. A reducer module for each detector provides functionality to create summary histograms.

## 2.4 Testing

MAUS has a set of tests at the unit level and the integration level, together with code-style tests for both Python and C++. Unit tests are implemented to test a single function, while integration tests operate

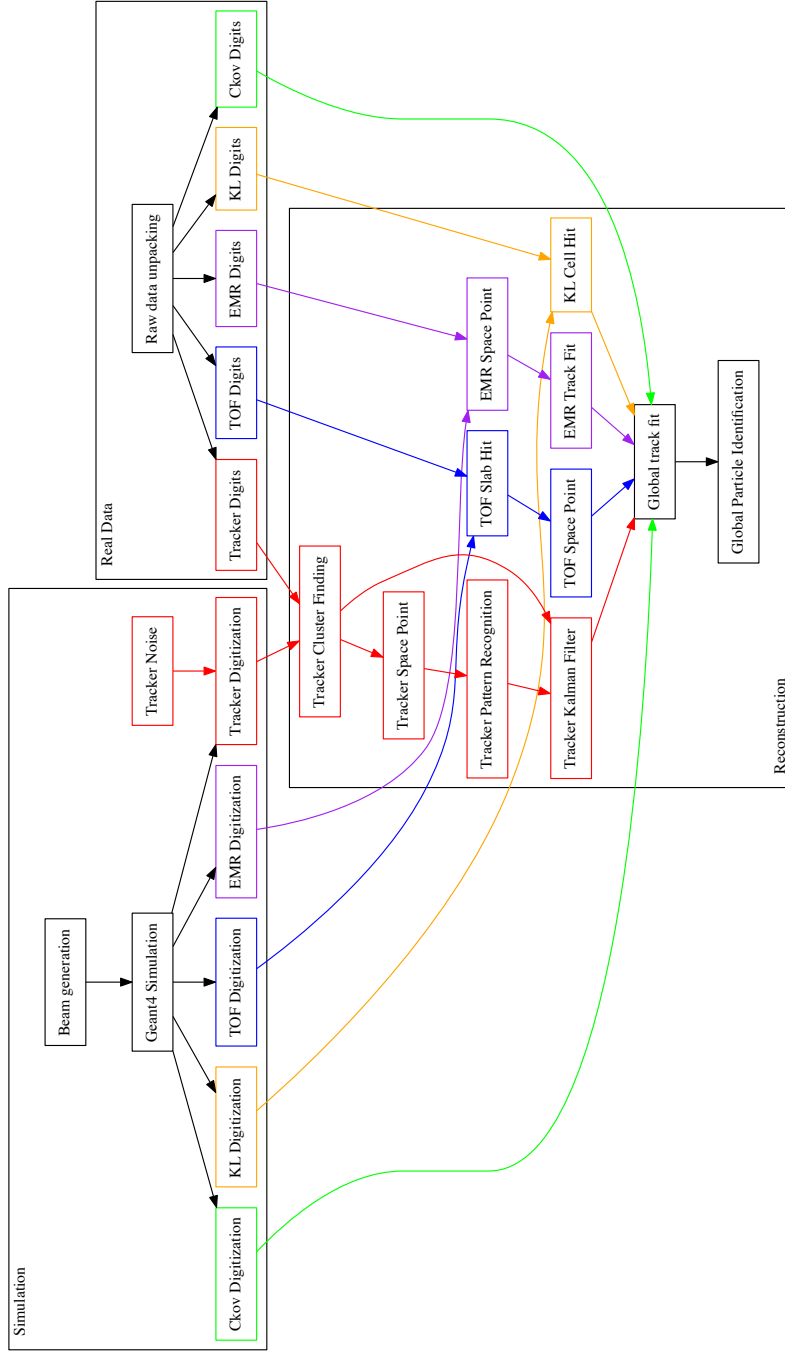


**Figure 11.** Data flow for the MAUS project. The data flow is color-coded by detector: Ckov - green, EMR - purple, KL - orange, TOF - blue, Tracker - red.

155 on a complete workflow. Unit tests check that each function operates as intended by the developer.  
156 Tests are run automatically for every version committed to the repository and results show that a high  
157 level of code coverage has been achieved. Integration tests allow the overall performance of the code  
158 to be checked against specifications. The MAUS team provides unit test coverage that executes 70–80  
159 % of the total code base. This level of coverage typically results in a code that performs the major  
160 workflows without any problems.

161 The MAUS codebase is built and tested using a Jenkins [23] continuous integration environment  
162 deployed on a cluster of servers. Builds and tests of the development branch are automatically triggered  
163 when there is a change to the codebase. Developers are asked to perform a build and test on a personal  
164 branch of the codebase using the test server before requesting a merge with the development trunk.  
165 This enables the MAUS team to make frequent clean releases. Typically MAUS works on a 4–8 week  
166 major-release cycle.

## 167 **3 Monte Carlo**

168 A Monte Carlo simulation of MICE encompasses beam generation, geometrical description of detectors  
169 and fields, tracking of particles through detectors and digitization of the detectors' response to particle  
170 interactions.

### 171 **3.1 Beam generation**

172 Several options are provided to generate an incident beam. Routines are provided to sample particles  
173 from a multivariate Gaussian distribution or generate ensembles of identical particles (pencil beams).  
174 In addition, it is possible to produce time distributions that are either rectangular or triangular in  
175 time to give a simplistic representation of the MICE time distribution. Parameters, controlled by  
176 datacards, are available to control random seed generation, relative weighting of particle species and  
177 the transverse-to-longitudinal coupling in the beam. MAUS also allows the generation of a polarized  
178 beam.

179 Beam particles can also be read in from an external file created by G4Beamline [24] or ICOOL  
180 [25], as well as files in user-defined formats. In order to generate beams which are more realistic  
181 taking into account the geometry and fields of the actual MICE beamline, we use G4Beamline to  
182 model the MICE beamline from the target to a point upstream of the second quad triplet (upstream  
183 of Q4). The beamline settings, *e.g.*, magnetic field strengths and number of particles to generate, are  
184 controlled through data-cards. The magnetic field strengths have been tuned to produce beams that  
185 are reasonably accurate descriptions of the real beam. Scripts to install G4beamline are shipped with  
186 MAUS.

187 Once the beam is generated, the tracking and interactions of particles as they traverse the rest of  
188 the beamline and the MICE detectors are performed using Geant4.

### 189 **3.2 Geant4**

190 The MICE Muon Beam line [4] consists of a quadrupole triplet (Q123) that captures pions produced  
191 when the MICE target intersects the ISIS proton beam, a pion-momentum-selection dipole (D1), a

192 superconducting solenoid (DS) to focus and transport the particles to a second dipole (D2) that is used  
193 to select the muon-beam momentum, and a transport channel composed of a further two quadrupole  
194 triplets (Q456 and Q789). The Geant4 simulation within MAUS starts 1 m downstream of the second  
195 beamline dipole magnet D2. Geant4 bindings are encoded in the Simulation module. Geant4 groups  
196 particles by run, event and track. A Geant4 run maps to a MICE spill; a Geant4 event maps to a  
197 single inbound particle from the beamline; and a Geant4 track corresponds to a single particle in the  
198 experiment.

199 GEANT provides a variety of reference physics processes to model the interactions of particles  
200 with matter. The default process in MAUS is “*QGSP\_BERT*” which causes Geant4 to model hadron  
201 interactions using a Bertini cascade model up to 10 GeV/c [26]. MAUS provides methods to set up  
202 the Geant4 physical processes through user-controlled data-cards. Finally, MAUS provides routines  
203 to extract particle data from the GEANT tracks at user-defined locations.

### 204 3.3 Geometry

205 MAUS uses an online Configuration Database to store all of its geometries. These geometries have  
206 been extracted from CAD drawings which are updated based on the most recent surveys and technical  
207 drawings available. The CAD drawings are translated to a geometry-specific subset of XML, the  
208 Geometry Description Markup Language (GDML) [27] prior to being recorded in the configuration  
209 database through the use of the FastRAD [28] commercial software package.

210 The GDML formatted description contains the beamline elements and the positions of the detector  
211 survey points. Beam-line elements are described using tessellated solids to define the shapes of the  
212 physical volumes. The detectors themselves are described using an independently generated set of  
213 GDML files using Geant4 standard volumes. An additional XML file is appended to the geometry  
214 description that assigns magnetic fields and associates the detectors to their locations in the GDML  
215 files. This file is initially written by the geometry maintainers and formatted to contain run-specific  
216 information during download.

217 The GDML files can be read via a number of libraries in Geant4 and ROOT for the purpose of  
218 independent validation. The files are in turn translated into the MAUS-readable geometry files either  
219 by directly accessing the data using a python extension or through the use of EXtensible Stylesheet  
220 Language Transformations (XSLT) [29].

### 221 3.4 Tracking, field maps and beam optics

222 MAUS tracking is performed using Geant4. By default, MAUS uses 4<sup>th</sup> order Runge-Kutta (RK4)  
223 for tracking, although other routines are available. RK4 has been shown to have very good precision  
224 relative to the MICE detector resolutions, even for step sizes of several cm.

225 Magnetic field maps are implemented in a series of overlapping regions. At each tracking step,  
226 MAUS iterates over the list of fields, transforms to the local coordinate system of the field map, and  
227 calculates the field. The field values are transformed back into the global coordinate system, summed,  
228 and passed to Geant4.

229 Numerous field types have been implemented within the MAUS framework. Solenoid fields can  
230 be calculated numerically from cylindrically symmetric 2D field maps, by taking derivatives of an



on-axis solenoidal field or by using the sum of fields from a set of cylindrical current sheets. Multipole fields can be calculated from a 3D field map, or by taking derivatives from the usual multipole expansion formulas. Linear, quadratic and cubic interpolation routines have been implemented for field maps. Pillbox fields can be calculated by using the Bessel functions appropriate for a TM010 cavity or by reading a cylindrically symmetric field map.

Matrix transport routines for propagating particles and beams through these field maps have been implemented. Transport matrices are calculated by taking the numerical derivative of the tracking output and can be used to transport beam ellipses and single particles.

The accelerator modeling routines in MAUS have been validated against ICOOL and G4Beamline and have been used to model a number of beamlines and rings, including a neutrino factory front-end [30].

### 3.5 Detector response and digitization

The modelling of the detector response and electronics enables MAUS to provide data used to test reconstruction algorithms and estimate the uncertainties introduced by detectors and their readout.

The interaction of particles in material is modeled using Geant4. A “sensitive detector” class for each detector processes Geant4 hits in active detector volumes and stores hit information such as the volume that was hit, the energy deposited and the time of the hit. Each detector’s digitization routine then simulates the electronics’ response to these hits, modeling processes such as the photo-electron yield from a scintillator bar, attenuation in light guides and the pulse shape in the electronics. The data structure of the outputs from the digitizers are designed to match the output from the unpacking of real data from the DAQ.

## 4 Reconstruction

The reconstruction chain takes as its input either digitized hits from the MC or DAQ digits from real data. Regardless, the detector reconstruction algorithms, by requirement and design, operate the same way on both MC and real data.

### 4.1 Time of flight

There are three time-of-flight detectors in MICE which serve to distinguish particle type. The detectors are made of plastic scintillator and in each station there are orthogonal  $x$  and  $y$  planes with 7 or 10 slabs in each plane.

Each Geant4 hit in the TOF is associated with a physical scintillator slab. The energy deposited by a hit is first converted to units of photo-electrons. The photo-electron yield from a hit accounts for the light attenuation corresponding to the distance of the hit from the photomultiplier tube (PMT) and is then smeared by the photo-electron resolution. The yields from all hits in a given slab are then summed and the resultant yield is converted to ADC counts.

The time of the hit in the slab is propagated to the PMTs at either end of the slab. The propagated time is then smeared by the PMT’s time resolution and converted to TDC counts. Calibration

267 corrections based on real data are then added to the TDC values so that, at the reconstruction stage,  
268 they can be corrected just as is done with real data.

269 The reconstruction proceeds in two main steps. First, the slab-hit-reconstruction takes individual  
270 PMT digits and associates them to reconstruct the hit in the slab. If there are multiple hits associated  
271 with a PMT, the hit which is earliest in time is taken to be the real hit. Then, if both PMTs on a  
272 slab have fired, the slab is considered to have a valid hit. The TDC values are converted to time  
273 and the hit time and charge associated with the slab hit are taken to be the average of the two PMT  
274 times and charges respectively. In addition, the product of the PMT charges is also calculated and  
275 stored. Secondly, individual slab hits are used to form space-points. A space-point in the TOF is a  
276 combination of  $x$  and  $y$  slab hits. All combinations of  $x$  and  $y$  slab hits in a given station are treated  
277 as space-point candidates. Calibration corrections, stored in the Configurations Database, are applied  
278 to these hit times and if the reconstructed space-point is consistent with the resolution of the detector,  
279 the combination is said to be a valid space-point. The TOF has been shown to provide good time  
280 resolutions at the 60 ps level [6].

## 281 4.2 Scintillating fiber trackers

282 The scintillating fiber trackers are the central piece of the reconstruction. As mentioned in Section 1.1,  
283 there are two trackers, one upstream and the other downstream of an absorber, situated within solenoidal  
284 magnetic fields. The trackers measure the emittance before and after particles pass through the absorber.

285 The tracker software algorithms and performance are described in detail in [31]. Digits are the  
286 most basic unit fed into the main reconstruction module, each digit representing a signal from one  
287 channel. Digits from adjacent channels are assumed to come from the same particle and are grouped  
288 to form clusters. Clusters from channels which intersect each other, in at least two planes from the  
289 same station, are used to form space-points, giving  $x$  and  $y$  positions where a particle intersected a  
290 station. Once space-points have been found, they are associated with individual tracks through pattern  
291 recognition (PR), giving straight or helical PR tracks. These tracks, and the space-points associated  
292 with them, are then sent to the final track fit. To avoid biases that may come from space-point  
293 reconstruction, the Kalman filter uses only reconstructed clusters as input.

## 294 4.3 KL calorimeter

295 Hit-level reconstruction of the KL is implemented in MAUS. Individual PMT hits are unpacked from  
296 the DAQ or simulated from MC and the reconstruction associates them to identify the slabs that were  
297 hit and calculates the charge and charge-product corresponding to each slab hit. The KL has been used  
298 successfully to estimate the pion contamination in the MICE muon beamline [32].

## 299 4.4 Electron-muon ranger

300 Hit-level reconstruction of the EMR is implemented in MAUS. The integrated ADC count and time  
301 over threshold are calculated for each bar that was hit. The EMR reconstructs a wide range of  
302 variables that can be used for particle identification and momentum reconstruction. The software and  
303 performance of the EMR are described in detail in [33].

## 304 **4.5 Cherenkov**

305 The CKOV reconstruction takes the raw flash-ADC data, subtracts pedestals, calculates the charge and  
306 applies calibrations to determine the photo-electron yield.

## 307 **4.6 Global reconstruction**

308 The aim of the Global Reconstruction is to take the reconstructed outputs from individual detectors and  
309 tie them together to form a global track. A likelihood for each particle hypothesis is also calculated.

### 310 **4.6.1 Global track matching**

311 Global track matching is performed by collating particle hits (TOFs 0, 1 and 2, KL, Ckovs) and  
312 tracks (Trackers and EMR) from each detector using their individual reconstruction and combining  
313 them using a RK4 method to propagate particles between these detectors. The tracking is performed  
314 outwards from the cooling channel – *i.e.*, the upstream tracker through TOF0, and downstream tracker  
315 through EMR. Track points are matched to form tracks using an RK4 method. Initially this is done  
316 independently for the upstream and downstream sections (*i.e.*, either side of the absorber). As the  
317 trackers provide the most accurate position reconstruction, they are used as starting points for track  
318 matching, propagating hits outwards into the other detectors and then comparing the propagated  
319 position to the measured hit in the detector. The acceptance criterion for a hit belonging to a track  
320 is an agreement within the detector’s resolution with an additional allowance for multiple scattering.  
321 Track matching is currently performed for all TOFs, KL and EMR.

322 The RK4 propagation requires the mass and charge of the particle to be known. Hence, it is  
323 necessary to perform track matching using a hypothesis for each particle type (muons, pions, and  
324 electrons). Tracks for all possible PID hypotheses are then passed to the Global PID algorithms.

### 325 **4.6.2 Global PID**

326 Global particle identification in MICE typically requires the combination of several detectors. The  
327 time-of-flight between TOF detectors can be used to calculate velocity, which is compared with the  
328 momentum measured in the trackers to identify the particle type. For all events but those with very  
329 low transverse momentum( $p_t$ ), charge can be determined from the direction of helical motion in the  
330 trackers. Additional information can be obtained from the CKOV, KL and EMR detectors. The global  
331 particle identification framework is designed to tie this disparate information into a set of hypotheses  
332 of particle types, with an estimate of the likelihood of each hypothesis.

333 The Global PID in MAUS uses a log-likelihood method to identify the particle species of a global  
334 track. It is based upon a framework of PID variables. Simulated tracks are used to produce probability  
335 density functions (PDFs) of the PID variables. These are then compared with the PID variables for  
336 tracks in real data to obtain a set of likelihoods for the PIDs of the track.

337 The input to the Global PID is several potential tracks from global track matching. During the  
338 track matching stage, each of these tracks was matched for a specific particle hypothesis. The Global  
339 PID then takes each track and determines the most likely PID following a series of steps:

- 340 1. Each track is copied into an intermediate track;

- 341 2. For each potential PID hypothesis  $p$ , the log-likelihood is calculated using the PID variables;
- 342 3. The track is assigned an object containing the log-likelihood for each hypothesis; and
- 343 4. From the log-likelihoods, the confidence level, C.L., for a track having a PID  $p$  is calculated and
- 344 the PID is set to the hypothesis with the the best C.L.

#### 345 **4.7 Online reconstruction**

346 During data taking, it is essential to visualize a detector's performance and have diagnostic tools  
347 to identify and debug unexpected behavior. This is accomplished through summary histograms of  
348 high and low-level quantities from detectors. The implementation is through a custom multi-threaded  
349 application based on a producer–consumer pattern with thread-safe FIFO buffers. Raw data produced  
350 by the DAQ are streamed through a network and consumed by individual detector mappers described in  
351 Section 3. The reconstructed outputs produced by the mappers, are in turn consumed by the reducers.  
352 The mappers and reducers are distributed among the threads to balance the load. Finally, outputs from  
353 the reducers are written as histogram images. Though the framework for the online reconstruction is  
354 based on parallelized processing of spills, the reconstruction modules are the same as those used for  
355 offline processing. A lightweight tool based on Django [34] provides live web-based visualization of  
356 the histogram images as and when they are created.

### 357 **5 Summary**

358 The MICE collaboration has developed the MAUS software suite to simulate the muon beamline,  
359 simulate the MICE detectors, and reconstruct both simulated and real data. The software also provides  
360 global track matching and particle identification capabilities. Simplified programming interfaces and  
361 testing environments enable productive development. MAUS has been successfully used to simulate  
362 and reconstruct data both online during data-taking and offline on batch production systems.

### 363 **Acknowledgments**

364 The work described here was made possible by grants from Department of Energy and National Science  
365 Foundation (USA), the Istituto Nazionale di Fisica Nucleare (Italy), the Science and Technology  
366 Facilities Council (UK), the European Community under the European Commission Framework  
367 Programme 7 (AIDA project, grant agreement no. 262025, TIARA project, grant agreement no.  
368 261905, and EuCARD), the Japan Society for the Promotion of Science and the Swiss National  
369 Science Foundation, in the framework of the SCOPES programme. We gratefully acknowledge all  
370 sources of support. We are grateful to the support given to us by the staff of the STFC Rutherford  
371 Appleton and Daresbury Laboratories. We acknowledge the use of Grid computing resources deployed  
372 and operated by GridPP [35] in the UK.

## References

- [1] T. Mohayai et al. First Demonstration of Ionization Cooling in MICE. In *Proc. 2018 International Particle Accelerator Conference, Vancouver*, 2018. FRXGBE3, <https://doi.org/10.18429/JACoW-IPAC2018-FRXGBE3>.
- [2] The IDS-NF collaboration. International design study for the neutrino factory: Interim design report, 2011. IDS-NF-020, [www.ids-nf.org/wiki/FrontPage/Documentation](http://www.ids-nf.org/wiki/FrontPage/Documentation).
- [3] Steve Geer. Muon Colliders and Neutrino Factories. *Annual Review of Nuclear and Particle Science*, 59:345 – 367, 2009.
- [4] M. Bogomilov et al. The MICE Muon Beam on ISIS and the beam-line instrumentation of the Muon Ionization Cooling Experiment. *JINST*, 7:P05009, 2012.
- [5] D. Adams et al. Characterisation of the muon beams for the Muon Ionisation Cooling Experiment. *Eur. Phys. J.*, C73(10):2582, 2013.
- [6] R. Bertoni et al. The design and commissioning of the MICE upstream time-of-flight system. *Nucl. Instrum. Meth.*, A615:14 – 26, 2010.
- [7] L. Cremaldi, D. A. Sanders, P. Sonnek, D. J. Summers, and J. Reidy, Jr. A cherenkov radiation detector with high density aerogels. *IEEE Trans. Nucl. Sci.*, 56:1475–1478, 2009.
- [8] M. Ellis, P.R. Hobson, P. Kyberd, J.J. Nebrensky, A. Bross, et al. The Design, construction and performance of the MICE scintillating fibre trackers. *Nucl. Instrum. Meth.*, A659:136–153, 2011.
- [9] R. Asfandiyarov et al. The design and construction of the MICE Electron-Muon Ranger. *JINST*, 11(10):T10007, 2016.
- [10] C. Tunnell and C Rogers. MAUS: MICE Analysis User Software. In *Proc. 2011 International Particle Accelerator Conference, San Sebastian*, 2011. MOPZ013.
- [11] <http://scons.org/>.
- [12] <https://bazaar.canonical.com>.
- [13] <http://launchpad.net>.
- [14] R. Brun and F. Rademakers. Root - an object oriented data analysis framework. *Nucl. Instrum. Meth.*, A389:81 – 86, 1997. <http://root.cern.ch/>.
- [15] S Agnostinelli et al. Geant4 - a simulation toolkit. *Nucl. Instrum. Meth.*, A506:250 – 303, 2003.
- [16] <https://scientificlinux.org>.
- [17] <https://centos.org>.
- [18] <https://getfedora.org>.
- [19] <https://ubuntu.com>.
- [20] J. Dean and S. Ghemawat. MapReduce: Simplified data processing on large clusters. In *Proceedings of OSDI04*, 2004. <http://research.google.com/archive/mapreduce.html>.
- [21] <http://json.org>.
- [22] <https://github.com/open-source-parsers/jsoncpp>.
- [23] <http://jenkins-ci.org>.

- 410 [24] Thomas J. Roberts and Daniel M. Kaplan. G4BeamLine programme for matter dominated beamlines. In  
411 *Proc. 2007 Particle Accelerator Conference, Albuquerque*, 2007. THPAN103.
- 412 [25] R. C. Fernow. Icool: A simulation code for ionization cooling of muon beams. In *Proc. 1999 Particle*  
413 *Accelerator Conference, New York*, 1999.
- 414 [26] J Apostolakis et al. Geometry and physics of the geant4 toolkit for high and medium energy applications.  
415 *Radiation Physics and Chemistry*, 78(10):859 – 873, 2009.
- 416 [27] J. McCormick R. Chytrcek. Geometry description markup language for physics simulation and analysis  
417 applications. *IEEE Trans. Nucl. Sci.*, 53:2892–2896, 2006.
- 418 [28] <http://fastrad.net>.
- 419 [29] <https://www.w3.org/standards/xml/transformation>.
- 420 [30] C.T Rogers et al. Muon front end for the neutrino factory. *Phys. Rev. ST Accel. Beams*, 16:040104, 2013.
- 421 [31] A. Dobbs, C. Hunt, K. Long, E. Santos, M.A. Uchida, P. Kyberd, C. Heidt, S. Blot, and E. Overton. The  
422 reconstruction software for the mice scintillating fibre trackers. *JINST*, 11(12):T12001, 2016.
- 423 [32] D. Adams et al. Pion Contamination in the MICE Muon Beam. *JINST*, 11(03):P03001, 2016.
- 424 [33] D. Adams et al. Electron-muon ranger: performance in the MICE muon beam. *JINST*, 10(12):P12012,  
425 2015.
- 426 [34] <https://www.djangoproject.com/>.
- 427 [35] [www.gridpp.ac.uk/](http://www.gridpp.ac.uk/).